L Schiesko et al.

# First experiments with Cs doped Mo as surface converter for negative hydrogen ion sources.

# First experiments with Cs doped Mo as surface converter for negative hydrogen ion sources.

L. Schiesko,[1, a)] G. Cartry,[2] C. Hopf,[1] T. Höschen,[1] G. Meisl,[1] O. Encke,[1] B. Heinemann,[1] K. Achkasov,[2, 3] P. Amsalem,[2] and U. Fantz[1]

[1)] *Max-Planck-Institut für Plasmaphysik, Boltzmannstrasse 2, D-85748 Garching, Germany*

[2)] *Aix Marseille University, CNRS, PIIM, UMR 7345, F-13013 Marseille, France*

[3)] *CEA-Cadarache, IRFM, F-13108 St Paul lez Durance, France*

(Dated: 5 May 2015)

A study was conducted on the properties of molybdenum implanted with caesium as an approach to reduce the Cs consumption of negative hydrogen ion sources based on evaporated Cs. The depth profiles of the implanted Cs were simulated by SDTrimSP and experimentally determined by XPS depth profiling. In particular, one year after implantation, the depth profiles showed no signs of Cs diffusion into the molybdenum, suggesting long term stability of the implanted Cs atoms. The $H^-$ surface generation mechanisms on the implanted samples in hydrogen plasma were investigated and the stability of the $H^-$ yield during four hours low power hydrogen plasma discharges was demonstrated. An estimation of the work function reduction (-0.8 eV) by the Cs implantation was performed and a comparison of the relative negative ion yields between the implanted samples and highly oriented pyrolitic graphite (HOPG) showed that the Cs doped Mo negative ion yield was larger.

## I. INTRODUCTION

The development of negative hydrogen ion sources is an active research topic covering many fields of application, as for example the proton synchrotron booster at CERN[1], neutron therapy[2], spallation neutron sources[3] as well as neutral beam injection (NBI) heating systems[4] for plasma experiments devices such as LHD[5] or JT60U[6].

The key component of ITER (International Thermonuclear Experimental Reactor) NBI is the negative hydrogen ion source. For heating and current drive, ITER requires the source to deliver 66 A of hydrogen and 57 A of deuterium negative ions, corresponding, for an extraction area of $0.2 \, m^2$, to $345 \, A/m^2$ and $285 \, A/m^2$ respectively. Moreover, the extracted beam should be homogeneous within 10 % and to minimize the stripping losses in the accelerator, the source has to operate at a pressure of 0.3 Pa. At this pressure, the negative ions are generated on a caesiated surface which is the first grid of the acceleration system (the plasma grid PG). Additionally, stable operation should be achieved during 1000 s in hydrogen and 1 h in deuterium[20]. The extraction of negative ions inevitably leads to the co-extraction of electrons. These electrons are filtered out of the beam by permanents magnets installed in the second grid of the extraction system, the extraction grid (EG). In order to avoid a too high power load of the filtered electrons on the EG, a current density ratio of co-extracted electron to negative ion lower than one must be achieved. At present, the amount of co-extracted electrons is the limiting source performance factor[8].

Since 2007 the prototype radio-frequency (RF) ion source for negative hydrogen ions[4,9,10], developed at Max-Planck-Institut für Plasmaphysik, Garching, is the ITER baseline design[11] for the Negative Neutral Beam Injection system (NNBI). The prototype ion source has an extraction area of 1/8 of the ITER ion source. The physical parameters required by ITER were achieved by the BATMAN test facility[4] which is dedicated to the ion source development and optimization as well as to the understanding of the physical processes due to its high flexibility and its large variety of diagnostics. The cw operation was demonstrated at the MANITU test bed (functionnally and technically identical to the BATMAN test bed), now decommissioned. Currently at IPP, the ELISE[8,12] test facility (1/2 area of the ITER ion source) is operated to demonstrate the scalability of the small size ion source prototype to larger areas. A full ITER area ion source is currently under construction at Consorzio RFX, Padua[13], as well as a complete beam line[14].

Due to its high current drive efficiency ($0.2$-$0.55 \times 10^{20} \, A/W/m^2$) NBI is also a key candidate as a heating and current drive (H&CD) system for a demonstration fusion power plant (DEMO)[15], an in particular for the case of a cw tokamak DEMO scenario for which a high driven current is mandatory.

Negative hydrogen ion sources are based on the conversion of neutral and positive hydrogen ion species ($H^0 / D^0$ and $H_x^+ / D_x^+$, x = 1...3) into negative ions $H^- / D^-$ on a converter surface. The negative ion generation yield is greatly enhanced by the evaporation of Cs[16–18] as it reduces the work function of the surfaces on which it is deposited. For IPP RF prototype sources, the source conditioning consists in the careful evaporation of fresh Cs, and typically leads to an increase

of the source performance: the extracted negative ion current increases while the amount of co-extracted electrons decreases (see for example[10]). The process of conditioning is delicate: the flux of injected Cs has to be carefully adjusted to maintain the performance of the source.

Laboratory experiments[19] confirmed what was experimetnally guessed when operating the prototype sources, i.e. that the high chemical reactivity of the surface deposited Cs layers with background gas components such as oxygen and water (impurities) led to a change of the properties of the Cs layers. Adsorption and absorption of impurities were shown to increase the work function[19], leading to a decrease of the source performance. A cleaning effect as well as a redistribution of the Cs during the plasma is observed[19], the two effects helping to reduce amount of fresh Cs having to be evaporated to maintain the source at a high performance. Nevertheless, the need to continuously evaporate fresh Cs in prototype sources is mainly due to the passivation of the already evaporated Cs by impurities[21,22] but also to the adsorption of Cs to locations which are less accessed by the plasma, leading to a lower redistribution of the Cs in those areas.

From an operational point of view, the Cs consumption of the negative hydrogen ion sources is a critical parameter because the maintenance of the source and Cs refilling procedures will strongly depend on it. In contrast to what can be expected by considering the vapor pressure of pure Cs, no substantial loss of Cs is observed. A quantitative assessment was performed for RF ion sources and most of the evaporated Cs was found in the sources with small traces on the grids[20,23]. For IPP RF prototype sources, the Cs consumption was determined to range between 5 and $10\,\mathrm{mg/h}$[15].

The first estimate of the ITER NBI Cs consumption was $7\,\mathrm{g}$ per half year[24]. The scaling of the Cs consumption to larger source size is arduous and not straightforward. A tentative estimate of the Cs consumption was proposed based on the measurements performed on the MANITU test facility: assuming an ITER-like DEMO source ($0.2\,\mathrm{m}^2$ extraction area, $60\,\mathrm{A}$ extracted current) this leads to $350$-$700\,\mathrm{g}$ for a DEMO injector operated $80\,\%$ of the year[15].

For IPP RF prototype sources, the Cs injection systems are based on small amounts (around $1\,\mathrm{g}$) of Cs stored in an oven. The refilling procedure of these ovens is routinely achieved and does not present any particular difficulty. For ITER the same Cs oven concepts will be used. In contrast, for DEMO a much larger storage is needed, as well as the development of a refilling procedure during operations which avoid a complete maintenance of the ion source. The Cs consumption of the source should also be the lowest possible to minimize the amount of activated Cs (evaporated Cs and Cs stored in the oven) by the hard neutron radiation coming from the tokamak. Even if the DEMO maintenance period is yet unknown, the removal of the accumulated Cs in the source is a drawback of the use of Cs ion sources.

It then appears clearly, from the different points evoked in the previous paragraphs, that a reduction of the Cs consumption can only be beneficial to operate the negative hydrogen ion sources at high performance.

Alternatives to Cs is currently an active research topic[21,22,25–27]. The main goal is to operate a Cs free negative ion source with a performance at least comparable to the caesiated sources. To this aim one must find or develop a converter surface with a negative hydrogen ion yield comparable to cesiated surfaces currently used in negative ion sources and which has to keep its properties stable for a long time, i.e. real cw operation. Candidates such as lanthanum hexaboride[21,22], diamond and boron doped diamond (BDD)[25] as well as highly oriented pyrolitic graphite (HOPG)[26,27] are interesting materials, some of them already showed that one could generate $H^-$ / $D^-$ ions. On HOPG, the $H^-$ / $D^-$ surface generation mechanisms in hydrogen plasma were already investigated[26–28]. These surface mechanisms are also expected as $H^-$ surface generation mechanisms in NNBI prototype sources.

Here it is proposed to study the properties of Mo implanted with Cs as a surface converter material. Mo was chosen as substrate because the converter surface of the NNBI sources, the PG, are foreseen to be made of copper covered by molybdenum. Copper is used for its excellent thermal properties when compared to other metals. Copper is covered by Mo in order to avoid Cu self sputtering during plasma phase. By implanting Cs into Mo, one expects to modify the surface properties of the Mo in order to have a stable compound with a reduced work function. One of the mile stones of this proposal is to dope the Mo in a way to obtain a material with a work function significantly lower than pure Mo, the ultimate goal being to obtain a material with a stable work function lower or as close as possible to what was measured in laboratory experiments when evaporating Cs on Mo substrates ($2.8\,\mathrm{eV}$ in vacuum, non measurable during plasma)[21]. If the work function reduction is not sufficient to operate NNBI sources in a Cs free environment, it is expected that working during plasma operations with a PG work function lower than pure Mo will lead to a decrease of the Cs consumption of NNBI sources, which in turn will ease the operations by shortening the conditioning and reconditioning processes. Reducing the Cs needed to operate the sources at high performance may lead to a higher stability and reproducibility of the extracted currents during long pulses[22] as well as a reduction of the Cs storage size for DEMO-like ion sources. A smaller amount of evaporated Cs in DEMO-like ion sources will also lead to less frequent maintenance and Cs storage refill.

Several studies already showed that Cs implanted into Mo led to a reduction of the work function[29–32]. In their work Tompa, Carr and Seidl investigated the work function changes by varying the dose and energy (up to 1 keV) of the $Cs^+$ ions impinging a Mo surface. It was observed that increasing the energy of the $Cs^+$ ions led to a decrease of the coverage as the ions become implanted more deeply[29,30]. Depth profiles were also analytically computed, via a simple model, with and without diffusion of the Cs into the Mo lattice. Sputter profiling showed evidence of diffusion[30,31]. Interestingly, the maximum decrease of the work function (- 2.6 eV) was observed for a surface coverage of 60 % (0.6 mono layers)[29,30], which is in good agreement with other measurements where the minimum was found between 40 % and 60 %[33]. For low coverage of the surface by Cs, the interaction of Cs atoms with crystalline Mo can be accurately described by density functional theory[34]. The authors show that a dipole effect induced by the interaction of the Cs and Mo atoms reduces the work function and is most effective for a Cs coverage between 40 % and 60 %, corresponding to 0.4 to 0.6 mono layers.

Several properties are nevertheless required in order to use Cs doped Mo compound as surface converter for negative ion sources. Among them, the long term stability (year scale) of the implanted Cs atoms must be proven. The stability and the reproducibility of the extracted currents during long cw hydrogen and deuterium plasmas must be demonstrated. The recovery of the negative ion yield after venting the source is also important.

In this paper, in order to provide a proof of principle for the use of Cs doped Mo compounds as surface converters and to reduce the implantation costs, very small amounts of Cs were implanted in Mo samples in order to obtain a surface Cs atomic fraction in the order of several percents and to constitute a near surface reservoir, the details of which will be given below. The first part of this paper is dedicated to the modeling of the implantation with SDTrimSP in order to determine the energy and dose of Cs required for reaching the requested atomic fractions and the constitution of the near surface reservoir. This section also presents experimental results obtained by XPS-depth profiling performed a few days and one year after implantation. The second part is dedicated to the description of the plasma reactor in which the samples are tested and the experimental results. In particular, the surface negative ion generation mechanisms in hydrogen plasma are identified, and the recovery of the relative negative ion yield after venting the source is discussed. Moreover the stability of the relative $H^-$ yield during 4 h cw operation is demonstrated and an estimate of the work function reduction induced by the implanted Cs atoms is given. Finally, a comparison of the relative negative ion yield between the implanted samples, pure Mo and HOPG[26–28] is presented.

## II. SDTRIMSP PROGRAM AND XPS-DEPTH PROFILING

In order to achieve a surface Cs concentration in the order of several percents and to constitute a near surface reservoir, the implantation profiles were computed by SDTrimSP[35–37]. SDTrimSP is based on the static TRIM.SP[38] and the dynamic TRIDYN[39,40]. SDTrimSP models atomic collisions in amorphous targets to calculate ranges, sputtering and reflexion yields, depth distribution of implanted atoms, as well as energy distributions of backscattered and sputtered atoms. The binary collision approximation is used to handle the atomic collisions. The trajectories of both incident ions and the recoil atoms are treated as series of collisions. In the static case, the target composition is fixed during the simulation. In the dynamic case, modifications of the composition of the target by ion bombardment are taken into account and the target composition is updated regularly. Diffusion and segregation are not included in the calculations.

Among several combinations of ion doses and energies tested as input parameters for SDTrimSP it was chosen to implant the samples in a two-step sequence and with a very small total dose of $10^{16}$ cm$^{-2}$ caesium atoms: first, a dose of $5.10^{15}$ cm$^{-2}$ caesium atoms at 15 keV followed by $5.10^{15}$ cm$^{-2}$ at 10 keV.

The choice of a two-step implantation sequence was motivated by the need to build up a near surface reservoir of Cs over several nanometers combined with a fair surface atomic fraction. The beneficial effect that is expected from a near surface reservoir of Cs is to mitigate a decrease of the surface Cs concentration due to diffusion into the bulk. The Cs reservoir is expected to prevent an unwanted slow increase of the work function with time by increasing the near surface available Cs atoms to maintain the work function at a low level for an extended period of time.

To this aim, the first sequence at 15 keV is needed in order to implant the Cs deeply into the samples. However the drawbacks of implanting at 15 keV are a high total sputtering yield leading to a poor surface and bulk Cs atomic fraction. The second sequence at a lower energy of 10 keV permits an increase of the surface and the near surface (2 - 3 nm below the surface) Cs concentration. The already implanted Cs increases the bulk material stopping power, while the reduction of the implantation energy down to 10 keV decreases both the total (and partial) sputtering yields and the implanted depth. In figure 1a, the depth profile was computed by SDTrimSP in dynamical mode for $5.10^{15}$ cm$^{-2}$ caesium atoms at 15 keV followed by $5.10^{15}$ cm$^{-2}$ caesium atoms at 10 keV with an implantation angle for the ions of 45 ° with respect to the normal incidence respectively. The incidence angle of the Cs atoms simulates the roughness of the samples and was treated as a free parameter. It can be thought of as the effective mean value of the
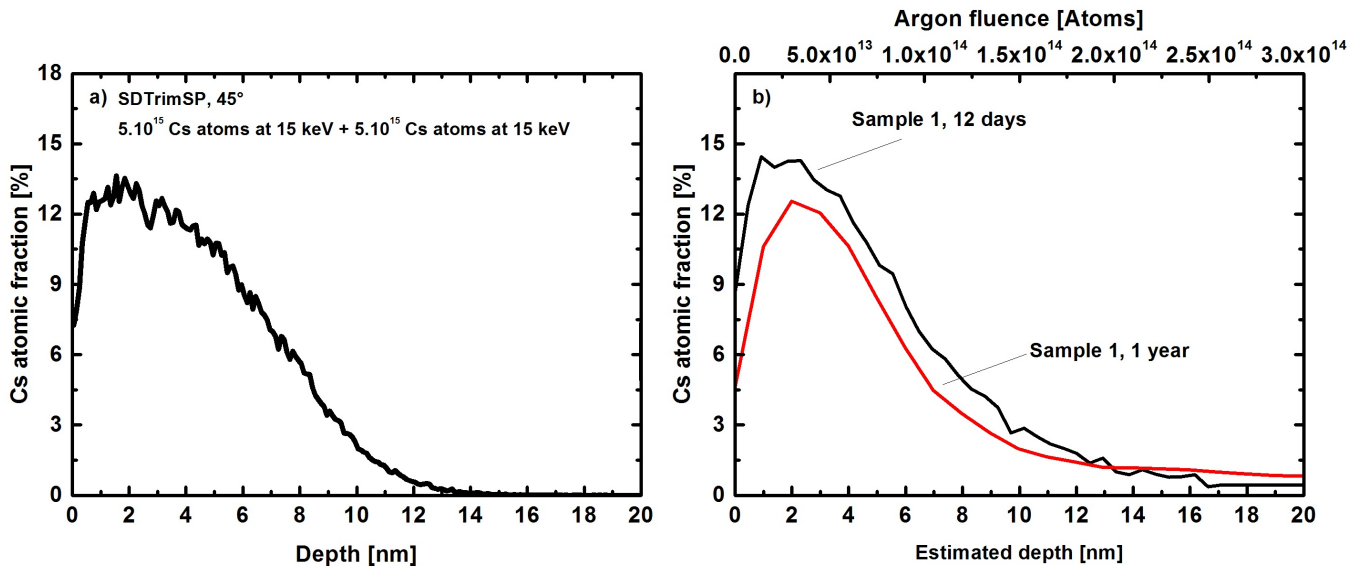
FIG. 1. a) Caesium atomic fraction computed with SDTrimSP for a 45 ° incidence angle, b) XPS depth profiling performed twelve days and one year after implantation versus the argon atoms fluence (top scale) and versus an estimated depth (bottom scale).

microscopic angle with the rough surface.

The samples were made of 99.95 % polycristalline Mo for a size of 1 cm$^2$ and were implanted by an external company according to the dose and energies previously described. The samples temperature was lower than 100 °C during the whole implantation process. For this proof of principle the samples were not polished prior to implantation. Profilometry showed a peak-to-peak surface structure prior to and after implantation of 0.8 $\mu$m. No post implantation annealing was performed. After implantation all the samples were maintained in air during five days. Sample 1 was then maintained under ultra high vacuum ($10^{-10}$ mbar), the other four under primary vacuum ($10^{-2}$ mbar).

The samples were analyzed by X-ray photoelectron spectroscopy (XPS) depth profiling using a PHI 5600 ESCA system with hemispherical analyzer in the constant analyzer energy mode. Spectra were recorded at a pass energy of 23.5 eV with a step width of 0.1 eV, using a standard X-ray source with Mg Ka radiation (1253.6 eV). The analysis area was determined by the Omnifocus lens to a spot with a diameter of 400 $\mu$m (150 $\mu$m for the first measurement series). Depth profiling was done by scanning a 10 keV Ar$^+$ ion beam over an area sufficiently larger than the measurement spot (Atomica WF 421 Microfocus Ion Gun).

The first part of this study was dedicated to the stability of the implanted Cs with time for samples stored at room temperature (either in air or vacuum), and not exposed to hydrogen plasma.

Figure 1b shows the Cs atomic fraction obtained by XPS-depth profiling performed on the same sample twelve days and one year after implantation: the lower scale shows the profile as a function of the argon fluence, while the upper scale is a rough estimation of the depth derived from the measured fluence, and from the sputtering yield by Ar and the areal density of the implanted sample both parameters being obtained by SDTrim.SP simulations. The measurements were performed at two different locations. For these two curves the measured intensities were converted to a Cs atomic fraction via sensitivity factors. The surface caesium concentration is of the order of 5 % (0.05 monolayer). One can clearly distinguish the Cs reservoir between 1 and roughly 4 nm. In figure 1b, the difference in amplitude observed between the measurement performed twelve days and one year after implantation seems to be explained by the fact that samples were not polished and the that the two different locations where the measurements were performed may have different roughness. As XPS depth profiling is a destructive method, using the same location on the sample for two different measurements is not possible. The hypothesis of roughness is supported by the fact that several other depth profiles of this particular sample were performed regularly (results not shown here), the magnitude of the Cs concentration and the shape of the intermediate profiles still being in the range of the results presented in figure 1b. Moreover, diffusion profiles typically show a decrease of the maximum concentration height as well as a broadening of the distribution, which is not the case. The last argument is supported by the similar shape of the normalized depth profiles (not shown here).

The depth profiles obtained by SDTrimSP are indicative, and cannot be compared to the experimental results determined by XPS depth profiling, despite

the good agreement, because Ar erosion and ion beam mixing induced by the Ar sputtering during XPS-depth profiling are not taken into account.

For this reason, forward modeling based calculations will be performed during the next experimental campaign[41] in order to include the ion beam mixing effect[41] and to improve the accuracy of the simulated depth profiles.

From the results presented in figure 1b, one can conclude that the implanted Cs is particularly stable for samples stored at room temperature, either in air or vacuum. Surface roughness is the probable reason explaining the discrepancy observed between XPS depth profiling performed twelve days and one year after implantation. Polished samples will be used during the next campaign in order to see whether or not a better agreement between the experimental profiles on the same samples can be obtained. Moreover, forward modeling based calculations will be performed to compare experimental and simulated depth profiles.

## III. EXPERIMENTAL SETUP, RESULTS AND DISCUSSION

### A. Experimental setup

The plasma experiments were performed with an ECR reactor[42] based on a modified Helicon source and presented in figure 2a. The microwave ECR source is from Boreal Plasma and was operated at 2.45 GHz. A more detailed description of the ECR source can be found in[43]. The reactor is equipped with a quadrupole mass and energy spectrometer (QMS) Hiden EQP 300. The tuning of the QMS was an important aspect of this study. For each sample bias the same tuning of the QMS was used in order to ensure a constant transmission function.

An RF-compensated movable Langmuir probe from STRAATUM was used to determine the electron and positive ion densities, the plasma and floating potentials as well as the electron temperature. The base pressure was $10^{-7}$ mbar. Typically the discharge parameters were 0.3 Pa hydrogen pressure, 100 W of injected power resulting in a positive ion density (electron density) of $3.10^{14}\,\mathrm{m}^{-3}$, a plasma potential of 6 V, an electron temperature of 0.5 eV and a dissociation degree $nH/nH_2$ of 1 % in the sample vicinity. The plasma composition determined by the QMS showed that it was largely dominated by $H_3^+$ with a proportion of 63 % followed by $H^+$ with 28 % and by $H_2^+$ with 9 %. A thermocouple placed at the back of the sample allowed for sample temperature measurements. The samples can be heated by driving a current in a thermocoax resistor placed behind the sample, and the sample holder can be rotated. Only one implanted sample was used during all the plasma experiments.

Figure 2b presents the sample and QMS arrangement. Typically, a sample bias ($V_s$) lower than the plasma potential ($V_p$) is applied to the sample while the QMS nozzle is grounded. The positive ions are attracted by the potential difference $V_0 = (V_{pl} - V_s)$ and strike the sample, while the negative ions created on the surface are repelled by the same potential difference and collected by the QMS where they are analyzed according to their energy. Under this bias configuration, the surface-produced negative ions are self-extracted from the plasma. The plasma potential being higher than the QMS nozzle potential no negative ion generated in the plasma volume can be extracted.

The distance between the mass spectrometer and the sample was 67 mm. At 0.3 Pa, the mean free path for stripping of a negative ion by collision with $H_2$ is also much larger than the QMS - sample distance[42,44]. One can then conclude that the negative ion losses on their way to the mass spectrometer are negligible.

### B. Negative ion generation mechanisms

Because of the thermal equilibrium between the positive ions and the neutrals in the plasma, the positive ions $H_x^+$ (x = 1...3) strike the sample surface with an energy $E_0 = e(V_{pl} - V_s)$ and are neutralized upon impact. As described in[42] the mass spectrometer measures the total kinetic energy of the negative ions:

$$E_T = E_{ki} + e(V_{pl} - V_s) - eV_{pl} \qquad (1)$$

with $E_{ki}$ being the energy at which a negative ion was created on the surface. On the right-hand side, the second term of eq. (1) is the energy difference between the sample and plasma potentials leading to an acceleration directed toward the QMS for the surface created negative ions, the third term acting as a deceleration for the negative ions due to the QMS nozzle being grounded (see figure 2b for a sketch of the potentials). For a constant sample bias, all the surface created negative ions will experience the same

$$E_r = e(V_{pl} - V_s) - eV_{pl} \qquad (2)$$

As a consequence, the key parameter to determine the surface generation mechanisms is the surface creation energy $E_{ki}$.

Two $H^-$ surface generation mechanisms are expected[26–28,45]: the backscattering of a positive ion ($H_x^+$, x = 1...3) or a neutral $H^0$ as $H^-$ and the sputtering of an adsorbed hydrogen as a negative ion by an incident positive ion.

Let us first consider the backscattering mechanism for a proton that looses no energy when interacting with the surface. The proton will be accelerated toward the
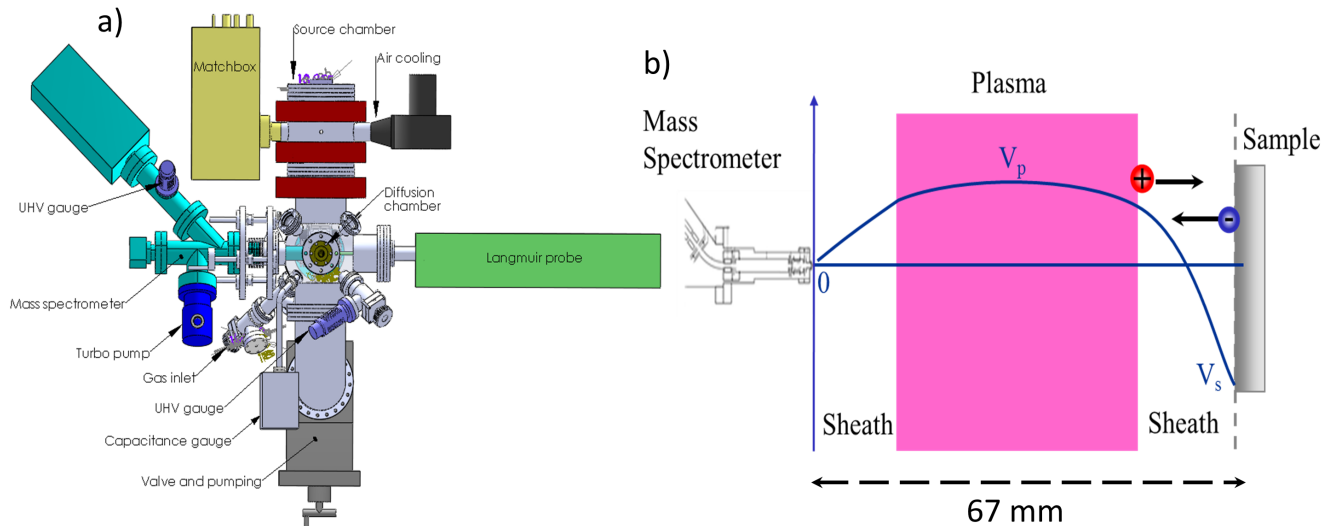
FIG. 2. a) Sketch of the ECR reactor test bed[42], b) sample - mass spectrometer arrangement, $V_s$ and $V_p$ are the sample and plasma potential respectively.
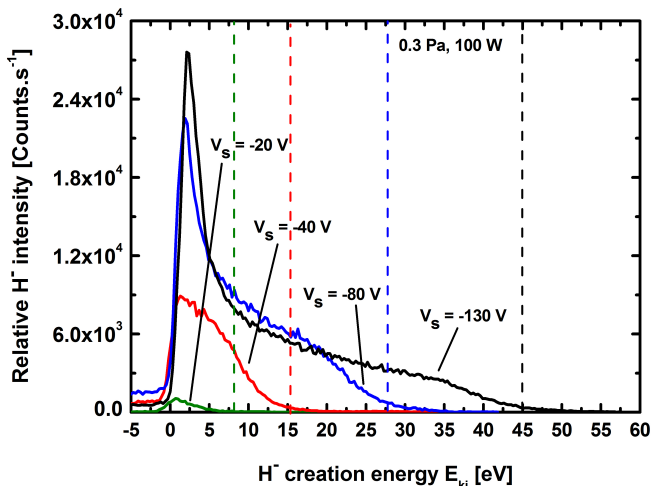


FIG. 3. $H^-$ creation energy $E_{ki}$ for a sample bias of -20 V, -40 V, -80 V, -130 V for a 0.3 Pa $H_2$, 100 W plasma. The dashed lines correspond to $E_0/3$ for each sample biases.

already neutral, capture only one electron.

Molecular ions are dissociated upon impact on the surface, the total kinetic energy of the ion being evenly splitted between the fragments. Assuming again an elastic backscattering, the maximum creation energy of a negative ion coming from $H_2^+$ and $H_3^+$ ion will be $E_2 = E_0/2$ and $E_3 = E_0/3$ respectively.

The second mechanism is the sputtering of an adsorbed hydrogen as a negative ion by an incident positive ion. SDTrimSP simulations were run to determine the outgoing energy of the H sputtered by the positive ions. Some approximations had to be done: the plasma being mainly made of $H_3^+$ which is dissociated upon impact, the energy of the impinging ions for each sample bias was then $E_0/3$ and their mass 1 a.m.u. It was found that the most probable energy (peak) of the sputtered H was around 6 eV for a sample bias of -130 V (43 eV positive ion energy), 4 eV for a sample bias of -80 V (27 eV positive ion energy) and that for lower bias voltages the positive ion energy was below the sputtering threshold.

It then appears from the previous considerations that the energy $E_{ki}$ at which the negative ions are created on the surface depend on the generation mechanism.

For NNBI prototype sources, most of the negative ions are generated by low temperature neutrals $H^0$, the energy of the positive ions hitting the PG is around 1 eV[46]. As a consequence, the energy of the positive ions and neutrals hitting the PG is way below the sputtering energy threshold. Thus, in NNBI prototype sources, the backscattering is probably the dominant surface negative ion generation mechanism.

surface by the sheath potential drop and thus will gain $E_0$. After being neutralized by resonant electron capture prior to collision and then having captured a second electron the resulting $H^-$ will be repelled from the surface. In this particular case where one assumes an "elastic" backscattering on the surface $E_{ki}$ is equal to $E_0$ and is the maximum energy for a negative ion created from a proton. Because the proton is neutralized prior to collision, the described mechanism of the backscattering as $H^-$ for a proton is in any point similar for a $H^0$ coming from the bulk plasma and backscattered as a $H^-$. The only differences are that $H^0$ atoms are not accelerated by the sheath potential drop and, being

### C. Results and discussion

Figure 3 shows the measured relative intensity of the H$^-$ as a function of the creation energy E$_{ki}$ for sample biases down to -130 V.

For a sample bias of -80 V and -130 V one observes a main low energy peak followed by a high energy tail. The shape of the negative ion distribution functions are similar to the ones observed on HOPG[27,28]. The main peak is not present at lower sample biases which will be discussed below. Because the plasma composition is dominated by H$_3^+$, the dashed line corresponds to E$_0$/3 for each sample bias and was plotted to show that the high energy part of the distribution function is the contribution of the backscattering mechanism. One clearly observes in figure 3 that whatever the sample bias, the kinetic energy of the surface created negative ions almost vanishes after E$_0$/3, the small extension of the distribution function beyond E$_0$/3 being attributed to H$^-$ created from H$^+$ and H$_2^+$.

For sample biases equal to -40 V and -20 V one observes a reduction of the number of collected negative ions and a diminution of the height of the main peak. This is related to the sheath voltage drop and to the angular emission of the negative ions (results not presented here[47]). For a sample bias of -80 V or -130 V the negative ions see their trajectories modified by the large sheath voltage drop in comparison to their creation energy. Thus, and in particular for low E$_{ki}$, the negative ions leave the surface in a direction normal to the surface and can be collected by the QMS nozzle hole. On the other hand, when the sample bias is reduced, then less negative ions leave in normal direction, explaining the decrease of the signal for lower sample biases.

The fact that the most probable energy of the sputtered hydrogen atoms is a few eV whatever the sample bias is, suggests that the low energy main peak observed for sample biases lower or equal to -80 V in figure 3 is due to the sputtering of adsorbed hydrogen as H$^-$ by the impinging positive ions. Moreover, the fact that no main peak can clearly be distinguished for V$_s$ equal to -20 V and -40 V in figure 3 is in good agreement with the sputtering calculations showing that the threshold energy is not reached for such small V$_s$.

Nevertheless, in order to clearly show that the low energy peak is mainly due to sputtering, the sample was slowly heated up to 600 °C while V$_s$ was maintained at -80 V during a 0.3 Pa, 100 W plasma. Figure 4a presents the obtained H$^-$ creation energy for different intermediate temperatures, the reference room temperature measurement being the spectrum at 55 °C in figure 4a. One observes in figure 4a that up to 400 °C, the height of the main peak slowly diminishes with temperature while the high energy parts (E$_{ki}$ > 7 eV) still superimpose. At 500 °C and beyond the main peak signal has collapsed while one observes a decrease of the high energy part,

the H$^-$ signals still superimposing for E$_{ki}$ ≥ 20 eV. The slight decrease of the main peak for temperatures up to 400 °C can be attributed to the decrease of the H surface coverage when the temperature is increased, as already observed in[28] for HOPG.

Several studies examined the retention of hydrogen and deuterium in Mo[48–52]. It appears from these studies that the onset release temperature of hydrogen isotopes from Mo ranges from 0 °C to 700 °C. The different temperatures observed for the release of hydrogen species is correlated to the sample temperature during hydrogen implantation and to the hydrogen fluence. Concerning the results presented in this paper, it is clear that some hydrogen is implanted into the Mo when the sample is negatively biased, the fluence being anyway smaller than the ones used in[48–52]. It is then likely that the collapse of the H$^-$ low energy peak for sample temperatures larger than 400 °C is due to the release of the adsorbed and trapped H when the desorption temperature is reached, suggesting that the contribution of the low energy peak is mostly due to the sputtering process. As a consequence, in figure 4a, the H$^-$ signal observed on spectrum measured with a sample temperature greater than 400 °C can be attributed to the backscattering process because of the disappearance of most of the adsorbed hydrogen and because of the continuity of the H$^-$ signal over the full E$_{ki}$ range.

As suggested in[53], the release of hydrogen may not only influence the sputtering yield but also the (negative) ionization efficiency due to the change of the electronic properties of the material in contact with the plasma. This could then explain the decrease of the relative backscattering yield observed for sample temperatures beyond 400 °C.

Moreover, in figure 4a, one can conclude from the unmodified high energy part of the distribution function that:

- the H$^-$ backscattering yield is not temperature dependent up to 400 °C,

- up to 400 °C the backscattering mechanism is not dependent on the H surface coverage, as observed in a similar fashion on HOPG[27,28]. This suggests that the backscattering mechanism, among several parameters, largely depends on the work function.

With or without plasma, increasing a surface temperature is a known procedure used to clean the surface-adsorbed impurities such as water, oxygen etc... Because the adsorption of impurities was shown to increase the work function in Cs evaporated experiments[19], a cleaning of these impurities by an increase of surface temperature in hydrogen plasma would lead to an increase of the negative ion yield. Even if in the results presentered in this paper, the Cs is implanted and not evaporated, a decrease of the work function should also lead to an increase of the negative ion yield. The superimposition observed in figure 4a of the high energy
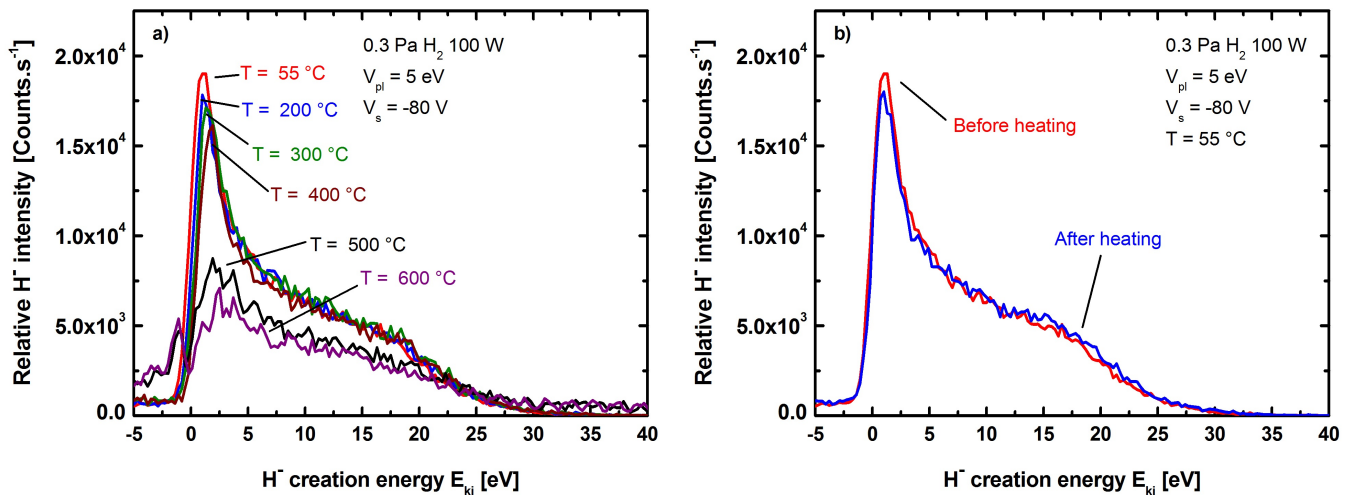
FIG. 4. a): H$^-$ creation energy E$_{ki}$ for a sample temperature of 55 °C, 200 °C, 300 °C, 400 °C, 500 °C, 600 °C and for a 0.3 Pa H$_2$, 100 W plasma and -80 V sample bias, b): H$^-$ creation energy for a sample temperature of 55 °C obtained before heating and after cooling phase.

parts (E$_{ki}$ > 7 eV) of the H$^-$ distributions, corresponding to the backscattering mechanism which depends on the work function, shows that up to 400 °C no particular cleaning effect is observed.

A question nevertheless arises from the results presented in figure 4a. The decrease in the relative negative ion yield corresponding to the contribution of the backscattering mechanism observed for E$_{ki}$ ≥ 7 eV beyond 400 °C in figure 4a could also be due to the diffusion of the Cs, leading to a change of the work function. Figure 4b compares the H$^-$ distribution functions obtained before heating the sample and after the cooling phase, both obtained during the same plasma shot and same sample bias. One can conclude from figure 4b, that the reappearance of the main low energy peak observed on the spectrum after cooling confirms that the sputtering is one of the low energy generation mechanism because the sample surface is again saturated by atomic hydrogen. Additionally, one can conclude that if Cs diffused because of the increased sample temperature, the variation of the depth profile and more importantly, the variation of the surface Cs concentration was small enough not to noticeably change the work function. This is confirmed by figure 5 where one can see that in comparison to the reference sample (kept at room temperature and never exposed to the plasma), that the depth profile of the sample heated and exposed to the plasma shows a lower maximum concentration and a broadening of the Cs distribution, which can be expected in cases of Cs diffusion. The diffusion of the Cs into the Mo sample is however marginal, and the surface Cs atomic fraction is almost identical to the reference sample, which is the probable reason of the stability of the relative H$^-$ yield prior to and after the sample heating.
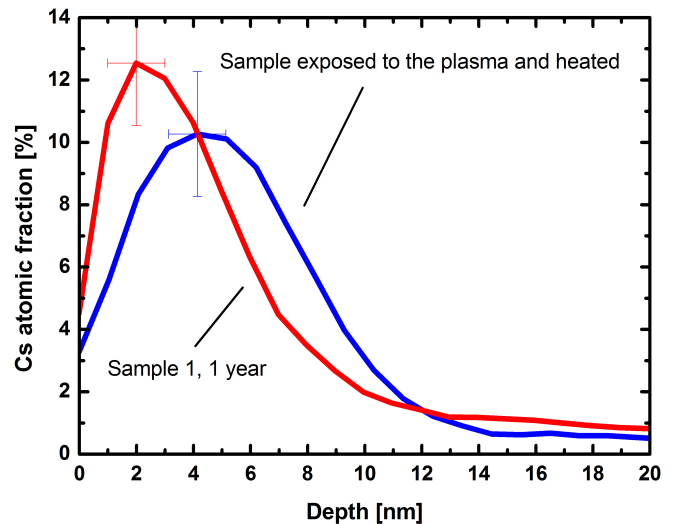


FIG. 5. Comparison of the depth profiles from the sample 1 (never exposed to the plasma) and the sample used during the plasma campaign.

The result presented in figure 5 is also a hint suggesting that the implementation of a near surface Cs reservoir can help in mitigating a decrease of the surface Cs atomic fraction. Nevertheless, the influence and possible mitigation offered by the presence of a near surface Cs reservoir on long term diffusion of the implanted Cs atoms should be further investigated.

The recovery of the negative ion yield after venting is an important aspect of this study. In Cs evaporated experiments, the Cs is passivated by air and fresh Cs has to be evaporated to recover a large negative ion yield. In the case of Cs doped Mo, one wanted to determine
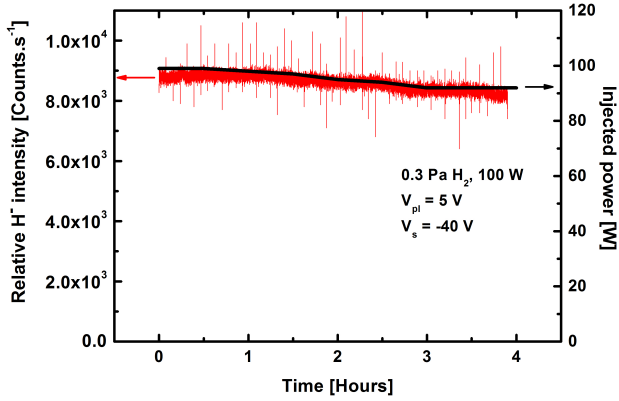
FIG. 6. Variation of the relative negative ion yield and of the injected power during 4 h operation.

whether or not it was possible to measure a comparable negative ion yield before and after venting the vessel, without evaporating fresh Cs. To this aim, the relative negative ion yield was recorded before and after having the vessel vented and for a sample maintained at room temperature. No evolution of the H⁻ yield could be observed from the start of the plasma after a vacuum of $10^{-7}$ mbar was achieved. This suggests that the plasma is probably able to quickly clean the surface of the adsorbed impurities. This fact is also supported by the results presented in figure 4a, which does not suggest any additional cleaning effect when the temperature of the sample is raised up to 400 °C.

In negative ion sources, long pulse cw operations (hour timescale) require a stable negative ion yield during the full pulse duration. The stability of the relative H⁻ yield during long cw plasma pulses is thus a critical aspect of this study. To this aim, the mass spectrometer was tuned to follow the height of the low energy main peak (which correspond to the sputtering process mainly, see figure 3 during 1 h 30 (not shown here) and 4 h cw plasma discharges. The plasma parameters and sample bias were kept constant during the full pulse duration in both cases.

Figure 6 presents the variation of the height of the main peak for a plasma pulse of 4 h at 0.3 Pa, 100 W of injected power and $V_s = $ -40 V. The sample temperature did not increase during the four hours. The slight decrease of the H⁻ signal (- 10 %) occurring after one hour is due to an observed decrease of the injected power also shown in figure 6 because of an increase of the reflected power. This small change in the matching is probably due to the warming up of the power supply, the RF transmission line and the matching box. Besides that, one can see in figure 6 that the relative ion yield is particularly stable over long pulse operations.

Figure 7a compares the relative negative ion yield

between a Cs doped Mo sample and a pure Mo sample both manufactured from the same raw material. The plasma parameters and sample bias were comparable and the mass spectrometer tuning rigorously identical for both cases in order to maintain the same transmission function. One observes clearly that even for around 5% Cs surface proportion, the relative negative ion yield of the Cs doped sample is much larger than the pure Mo sample. From the spectrum presented in figure 7a, one can give a rough estimate of the work function reduction induced by the implantation of Cs as will be discussed in the following.

It is known that the formation probability P⁻ to create negative ions on metals[54,55] (and references therein) is given by:

$$P^- \propto e^{-(\Phi - A)/\epsilon_n} \qquad (3)$$

with $\Phi$ being the work function of the converter surface, A the electron affinity of the neutral atoms and $\epsilon_n$ a parameter whose magnitude should fall in the range 0.5 - 1 eV and is thought to be dependent on the normal component of the ion velocity[56]. Experimental data[57,58] however showed that the parameter $\epsilon_n$ was largely indepedent of the ion velocity and in the range of 0.2 - 0.4 eV. Thus, based on the work function of pure Mo (4.6 eV)[59,60], it is possible to give a rough estimate of the work function change induced by the implantation of Cs. To this aim, one defines by $f_{Mo}(E)$ and $f_{Cs/Mo}(E)$ the experimentally measured H⁻ creation energy distribution functions obtained with pure Mo and Cs doped Mo samples respectively and shown in figure 7a. Furthermore, one defines by $I_{Mo} = \int_0^\infty f_{Mo}(E)\, dE$ and $I_{Cs/Mo} = \int_0^\infty f_{Cs/Mo}(E)\, dE$ the integrals of these distribution functions, as well as $R = \dfrac{I_{Cs/Mo}}{I_{Mo}}$ as the ratio of these integrals. Provided relation (3) it follows:

$$R = \frac{e^{-(\Phi_{Cs/Mo} - A)/\epsilon_n}}{e^{-(\Phi_{Mo} - A)/\epsilon_n}} \qquad (4)$$

and then

$$\Phi_{Cs/Mo} = \Phi_{Mo} - \epsilon_n \, ln(R) \qquad (5)$$

with $\Phi_{Cs/Mo}$ and $\Phi_{Mo}$ the work functions of the implanted probe and pure Mo respectively. The estimated work function $\Phi_{Cs/Mo}$ of the Cs doped Mo samples is then comprised between 3.8 for $\epsilon_n = 0.4$ and 4.2 $\epsilon_n = 0.2$ which corresponds to a work function reduction comprised between -0.8 and -0.4 eV. This result is in good agreement with other experiments[54,55,61] where the work function reduction induced by Cs coverage or implantation was measured. One can see that for only 0.05 monolayers of Cs, the reduction of the work
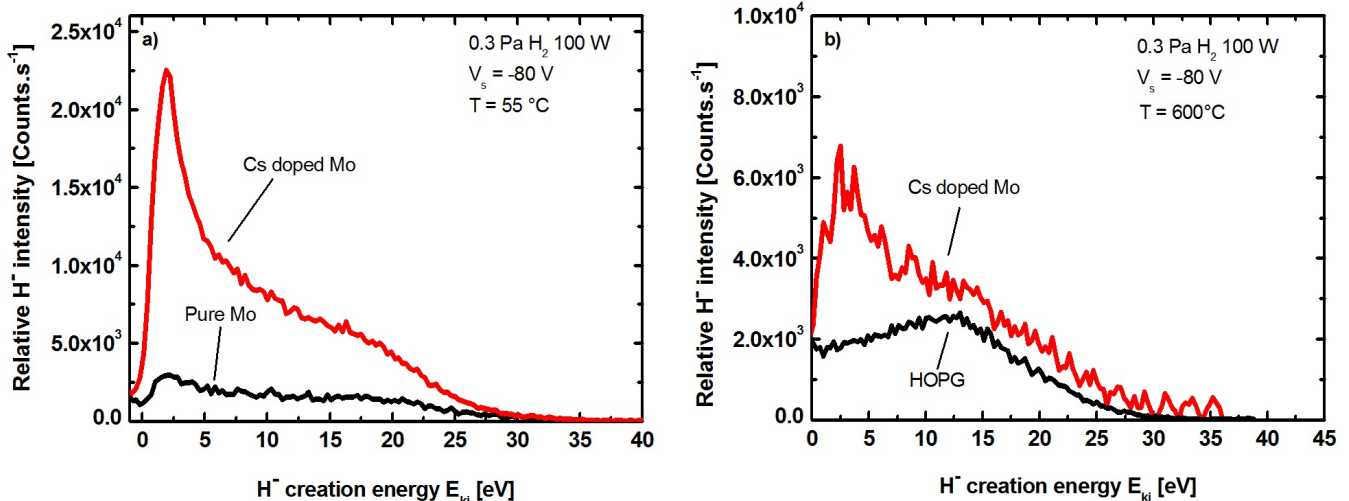
FIG. 7. a): comparison of the relative $H^-$ yield of a Cs implanted sample to pure Mo sample, b): comparison of the relative $H^-$ yield of a Cs implanted sample to an HOPG sample.

function is already non negligible. The work function of the Cs doped Mo samples will be measured in the future in order to confirm the previous estimate.

Figure 7b compares the relative $H^-$ ion yield of a Cs implanted sample to an HOPG sample both heated up at 600°C. Again, precautions were taken in order to have very close plasma parameters, same sample temperature and an identical QMS tuning for both samples. HOPG was chosen as a comparison sample because up to now it is a promising alternative to Cs candidate.
As previously mentioned, in NNBI prototype sources, the backscattering is probably the dominant surface generation mechanism. It was previously shown that at high temperature, most of the negative ions were generated from the backscattering mechanism (see[27,28] for HOPG). For this reason, figure 7b compares the relative yields at 600 °C, temperature for which most of the surface generated negative ions were created via the backscattering mechanism, which is mostly dependant of the work function.
One can clearly see in figure 7b that the negative ion yield of the HOPG is lower than the one observed for Cs-implanted samples, which make Cs doped Mo an interesting candidate for negative ion sources.

Future experiments will focus on different aspects. First, the surface Cs atomic fraction should be increased to determine whether or not the negative ion yield is increased, if the implanted Cs atoms are stable and if the results are reproducible. Second, a measure of the work function should be performed. Third, in this work the plasma flux was much lower than what can be expected in a negative ion NBI prototype source. The stability of the depth profiles of probes exposed to hydrogen plasmas with a much larger flux of positive ions and atoms should

be determined. Another interesting study to perform is also to compare the negative ion yield between Cs doped Mo samples and pure Mo samples covered by evaporated Cs.

## IV. CONCLUSION

In this paper, Mo samples were implanted by a very small dose of Cs leading to a surface Cs atomic fraction of roughly 5%, which corresponds to 0.05 monolayers. The goal was to test as a proof of principle the stability and material properties of this compound as an efficient surface converter to generate negative hydrogen ions. XPS depth profiling was performed regularly, showing a long term stability proved up to one year. The use of SDTrimSP allowed the calculation of the implanted depth profiles, whose results were in good agreement with the experimental profiles. The surface generation mechanisms were identified, similarly to a previous work on HOPG: the backscattering of the positive ions as negative ions was found to be the mechanism which gives rise to the high energy part of the negative ion creation energy function, while most of the low energy created negative ions are issued from the sputtering by positive ions as $H^-$ of an adsorbed H onto the surface. Temperature measurements permitted to show that Cs could diffuse into and probably outside of the Mo. Increasing the sample temperature up to 600 °C did not show an increase of the $H^-$ ion yield, meaning that no particular cleaning effect of the surface was occuring. Low surface temperature (below 400 °C) operation is to be preferred, to avoid the Cs diffusion. The recovery of the negative ion yield after venting was checked and the stability of the $H^-$ yield in plasma was confirmed several times and up to 4 h continuous operation. By comparing

the relative yields of the Cs doped samples and pure Mo samples it was possible to give an estimate of the work function of the implanted sample which ranges between 3.8 and 4.2 eV (4.6 eV for pure Mo). Finally a comparison with HOPG showed that the implanted samples had a larger yield.

[1] Lettry J. et al., Rev. Sci. Inst. 85, (2014) 02B122.
[2] Schmidt J. S., Koubek B., Schempp A., Tan C. Y., Bollinger D. S. et al., Phys. Rev. ST Accel. Beams 17, (2014) 030102 .
[3] Stockli M. P., Ewald K. D., Han B. X., Murray S. N. Jr. et al., Rev. Sci. Inst. 85, (2014) 02B137 .
[4] Speth E. et al., Nucl. Fus. 46 (2006) 220.
[5] Takeiri Y. et al., Nucl. Fusion 46, (2006) S199210.
[6] Kojima A. et al., Nucl. Fusion 51, (2011) 083049.
[7] Boilson D., Priv. comm. (2014).
[8] Fantz U. et al., Rev. Sci. Inst. 85, (2014) 02B305.
[9] Franzen P. et al., Nucl. Fus. 47 (2007) 264.
[10] Schiesko L. et al., Plas. Phys. & Cont. Fus. 53 (2011) 085029.
[11] Hemsworth R., Tanga A. and Antoni V., Rev. Sci. Inst. 79, (2008) 02C109.
[12] Bonomo F. et al., Plas. Phys. & Cont. Fus. 56 (2014) 015006.
[13] P. Sonato et al., Fusion Eng. Des. 84, (2009) 269.
[14] Chitarin G. et al., Rev. Sci. Instrum. 83 (2012) 02B107.
[15] Franzen P. and Fantz U., Fus. Eng. & Design 89, (2014) 2594.
[16] Belchenko Yu. I., Dimov G. I., and Dudnikov V. G., Nucl. Fus. 14 (1974) 113-114.
[17] Belchenko Yu. I., Dimov G. I., and Dudnikov V. G., Proc. Symp. Production and Neutralization of Negative Hydrogen Ions and Beams, Brookhaven, 1977 (BNL, Upton, NY, 1977).
[18] Belchenko Yu. I., Rev. Sci. Instrum. 64 (1993) 1385.
[19] Gutser R., Wimmer C. and Fantz U., Rev. Sci. Instrum. 82, (2011) 023506.
[20] Boilson D., Ellingboe A., Faulkner R., Hemsworth R., de Esch H., Krylov A. et al., Fus. Eng. Design 74 (2005) 295298.
[21] Fantz U., Gutser R. and Wimmer C., Rev. Scientific Instrum. 81 (2010) 02B102.
[22] Fantz U. and Wimmer C., Rev. Scientific Instrum. 83 (2011) 02B110.
[23] Krylov A., Boilson D., Fantz U., Hemsworth R., Provitina O., Pontremoli S. et al., Nucl. Fus. 46 (2006).
[24] Okumura Y., Fujiwara Y., Kashiwagi M., Kitagawa T. and K. Miyamoto, Rev. Sci. Instrum. 71, (2000) 1219.
[25] Kumar P., Ahmad A., Pardanaud C. et al., J. Phys. D: Appl. Phys. 44 (2011) 372002.
[26] Schiesko L. et al., Plasma Sources Sci. Technol. 17 (2008) 035023.
[27] Schiesko L., Carrère M., Layet J.-M. and Cartry G., Applied Phys. Lett. 95, (2009) 191502.
[28] Schiesko L., Carrère M., Layet J.-M. and Cartry G., Plasma Sources Sci. Technol. 19, (2010) 045016.
[29] Tompa G. S. et al., App. Phys. Lett 48, (1986) 1048.
[30] Carr W. et al., Journ. Vac. Sci. Tech. A 5, (1987) 1250.
[31] Tompa G. S. et al., Surf. Sci., 198, (1988) 431.
[32] Isakhanov Z. et al. Tech. Phys. 56, (2011) 546.
[33] Soukassian P. et al., Solid State Comm. 44, (1982) 1375.
[34] Chubb S. R. et al., Phys. Rev. B. 36, (1987) 4112.
[35] Eckstein W. et al., IPP Rep. 12/08, Max-Planck-Institut für Plasmaphysik, Garching (2007).
[36] Eckstein W. *Computer Simulation of Ion Solid Interactions, Springer Series in Materials Science*, 10, Springer, Berlin (1991).
[37] Eckstein W. et al., IPP Rep. 12/3, Max-Planck-Institut für Plasmaphysik, Garching (2007).
[38] Biersack J. P. and Eckstein W., App. Phys. A 34, (1984) 73.
[39] Möller W. and Eckstein W., Nucl. Inst. Meth. B 2, (1984) 814.
[40] Möller W., Eckstein W. and Biersack J. P., Comput. Phys. Comm. 51, (1988) 355.
[41] Meisl G et al., New J. Phys. 16, (2014) 093018.
[42] Ahmad A., Dubois J., Pasquet T., Carrère M., Layet J.-M., Faure J.-B., Cartry G., Kumar P., Mina T., Mochalskyy T. and Simonin A., Plasma Sources Sci. Technol. 22 (2013) 025006.
[43] Béchu S., Soum-Claude A., Bès A., Lacoste A., Svarnas P., Aleiferis S., Ivanov A. A. and Bacal M., Phys. Plasmas 20 (2013) 101601.
[44] Phelps A.V., J. Phys. Chem. Ref. Data 19 (1990) 653.
[45] Cartry G. et al., Phys. Plasmas 19 (2012) 063503.
[46] Wünderlich D., Schiesko L. et al., Plasma Phys. Control. Fusion 54, (2012) 125002.
[47] Schiesko L., Cartry G. et al., To be published.
[48] Haasz A.A. and Davis J. W., Journ. Nucl. Mat. 241-243, (1997) 1076.
[49] Tanabe T., Hachino H. and Takeo M., Journ. Nucl. Mat. 176-177, (1990) 666.
[50] Sakamato R., Muroga T. and Yoshida N., Journ. Nucl. Mat. 233-237, (1996) 776.
[51] Van Veen A. and Filius H. A., Journ. Nucl. Mat. 155-157, (1988) 1113.
[52] Causey R. A., Kunz C. L. and Cowgil D. F., Journ. Nucl. Mat. 337-339, (2005) 600-603.
[53] Ahmad A., Pardanaud C., Carrére M., Layet J.-M., Gicquel A., Kumar P., Eon D., Jaoul C., Engeln R. and Cartry G., J. Phys. Appl. Phys. 47, (2014) 085201
[54] Gnaser H., Phys. Rev. B 54 (1986) 16456.
[55] Kudriavtsev Y., Asomoza R., Appl. Surf. Sci. 167 (2000) 12.
[56] Lang N. D., Phys. Rev. B 27, (1983) 2019.
[57] Yu M. L., Phys. Rev. Lett 40, (1978) 574.
[58] Yu M. L., Phys. Rev. B 26, (1982) 4731.
[59] J. Scheer et al., Nucl. Instr. Meth. B 230, (2005) 330.
[60] P. Hughes, M. Coplan, J. DeFazio et al., J. Vac. Sci. Technol. A 27, (2009) 1188.
[61] Swanson L. W. and Strayer R. W., J. Chem. Phys. 48, (1968) 2421.